Clinical Cancer Research

A Novel Anti-CD22 Anthracycline-Based Antibody–Drug Conjugate (ADC) That Overcomes Resistance to Auristatin-Based ADCs

Shang-Fan Yu[1], Bing Zheng[1], MaryAnn Go[1], Jeff Lau[1], Susan Spencer[1], Helga Raab[1], Robert Soriano[1], Suchit Jhunjhunwala[1], Robert Cohen[1], Michele Caruso[2], Paul Polakis[1], John Flygare[1], and Andrew G. Polson[1]

Abstract

Purpose: We are interested in identifying mechanisms of resistance to the current generation of antibody–drug conjugates (ADC) and developing ADCs that can overcome this resistance.

Experimental Design: Pinatuzumab vedotin (anti-CD22-vc-MMAE) and polatuzumab vedotin (anti-CD79b-vc-MMAE) are ADCs that contain the microtubule inhibitor monomethyl auristatin E (MMAE) attached to the antibody by the protease-cleavable linker maleimidocaproyl-valine-citrulline-p-aminobenzoyloxycarbonyl (MC-vc-PAB). Early clinical trial data suggest that these ADCs have promising efficacy for the treatment of non-Hodgkin lymphoma (NHL); however, some patients do not respond or become resistant to the ADCs. Anthracyclines are very effective in NHL, but ADCs containing the anthracycline doxorubicin were not clinically efficacious probably due to the low drug potency and inadequate linker technology. The anthracycline analogue PNU-159682 is thousands of times more cytotoxic than doxorubicin, so we used it to develop a new class of ADCs. We used the same MC-vc-PAB linker and antibody in pinatuzumab vedotin but replaced the MMAE with a derivative of PNU-159682 to make anti-CD22-NMS249 and tested it for *in vivo* efficacy in xenograft tumors resistant to MMAE-based ADCs.

Results: We derived cell lines from *in vivo* xenograft tumors that were made resistant to anti-CD22-vc-MMAE and anti-CD79b-vc-MMAE. We identified P-gp (ABCB1/MDR1) as the major driver of resistance to the vc-MMAE–based conjugates. Anti-CD22-NMS249 was at least as effective as anti-CD22-vc-MMAE in xenograft models of the parental cell lines and maintained its efficacy in the resistant cell lines.

Conclusions: These studies provide proof of concept for an anthracycline-based ADC that could be used to treat B-cell malignancies that are resistant to vc-MMAE conjugates. *Clin Cancer Res; 21(14); 3298–306. ©2015 AACR.*

Introduction

Anthracyclines are one of the most widely used classes of chemotherapy. In particular, they are the cornerstone of treatment for aggressive non-Hodgkin lymphoma (NHL) and acute myeloid leukemia. Anthracyclines, such as doxorubicin, that are used in systemic therapy have not been clinically effective when used in the context of an antibody–drug conjugate (ADC), probably because the drugs were not sufficiently potent. The lack of potency may have been exacerbated by inadequate linker design (1). The current generation of ADCs that are showing clinical success uses drugs that are much more potent (2). Because there are no novel anthracycline-based ADCs currently in clinical development and this class of drugs has proven so effective in the treatment of a wide variety of cancers, an anthracycline-based ADC seems to be a promising approach to improve and broaden the utility of ADC technology. For these proof-of-concept studies, we focused on NHL as an indication because of its responsiveness to anthracyclines and promising clinical data with the current generation of ADCs. There are five ADCs in clinical development for the treatment of B-cell NHL, moxetumomab pasudotox (CAT-8015), pinatuzumab vedotin (DCDT2980S, anti-CD22-MC-vc-PAB-MMAE), polatuzumab vedotin (DCDS4501A, anti-CD79b-MC-vc-PAB-MMAE), SAR3419 (anti-CD19-SPDB-DM4), and SGN-CD19A (anti-CD19-MC-MMAF; ref. 3). Moxetumomab pasudotox is a recombinant immunotoxin composed of the Fv fragment of an anti-CD22 monoclonal antibody fused to a 38-kDa fragment of Pseudomonas exotoxin A, PE38 (4), and is under investigation for hairy cell leukemia (HCL) and NHL. Pinatuzumab vedotin and polatuzumab vedotin are anti-CD22 and anti-CD79b ADCs, respectively, with protease-sensitive maleimidocaproyl-valine-citrulline-p-aminobenzoyloxycarbonyl (MC-vc-PAB) linkers attached to the microtubule-disrupting agent monomethyl auristatin E (MMAE; refs. 5, 6). These ADCs have shown efficacy in heavily pretreated patients in phase I trials (6, 7) and are currently in phase II testing in combination with rituximab. SAR3419 consists of a humanized anti-CD19 antibody and a linker (SPDB) cleavable by disulfide reduction attached to the maytansinoid DM4 (a microtubule-disrupting agent) through lysine residues. Phase I trials of SAR3419 in

[1]Research and Early Development, Genentech Inc., South San Francisco, California. [2]Nerviano Medical Sciences, Nerviano MI, Italy.

Note: Supplementary data for this article are available at Clinical Cancer Research Online (http://clincancerres.aacrjournals.org/).

S.-F. Yu and B. Zheng contributed equally to this article.

Corresponding Author: Andrew G. Polson, Genentech Inc., 1 DNA Way, South San Francisco, CA 94080. Phone: 650-225-5134; Fax: 650-225-6240; E-mail: polson@gene.com

doi: 10.1158/1078-0432.CCR-14-2035

AACR

Translational Relevance

Antibody–drug conjugates (ADCs) are a technology for increasing the safety and efficacy of traditional chemotherapy. There are three ADCs in clinical trials for the treatment of non-Hodgkin lymphoma all of which contain microtubule inhibitors as the drug. While promising, clinical results show some patients do not respond or relapse during treatment. We show that an ADC based on a potent anthracycline can be effective in xenograft tumors that have innate or acquired resistance to the auristatin-based ADCs pinatuzumab vedotin and polatuzumab vedotin. Further, we identify P-gp as possible mechanism of resistance to the auristatin-based ADCs. One probable reason anthracycline-based ADCs have not been successful in the clinic is due to the use of drugs that lack the potency required for the ADC technology. Our findings provide a step forward in accessing this important class of chemotherapy as an ADC.

relapsed and refractory NHL have also shown clinical activity (8). SGN-CD19A, another ADC targeting CD19 but with a stable linker and a less membrane-permeable auristatin, has started early clinical trials in NHL. Despite this progress, some patients still do not respond to these ADCs, and others respond but progress while on treatment. In patients with relapsed or refractory B-cell NHLs, the objective response rates were 41%, 53%, and 30% for pinatuzumab vedotin, polatuzumab vedotin, and SAR3419, respectively (6, 7, 9). Understanding this resistance and developing methods to overcome it would help develop the next generation of ADCs for the treatment of NHL and other cancers.

Here, we show proof of concept for an anthracycline-based ADC for the treatment of NHL and demonstrate that our novel ADC is effective in xenograft models that have innate or acquired resistance to the microtubule inhibitor–based ADCs. In addition, we identify possible drivers of resistance to the vc-MMAE–based ADCs pinatuzumab vedotin and polatuzumab vedotin.

Materials and Methods

Antibodies and ADCs

Pinatuzumab vedotin (DCDT2980S, anti-CD22-MC-vc-PAB-MMAE) and polatuzumab vedotin (DCDS4501A, anti-CD79b-MC-vc-PAB-MMAE) were generated as previously described (5, 10). THIOMAB version of the anti-CD22 and anti-CD79b antibodies was generated as described (11). NMS249 was synthesized. Before conjugation of the THIOMAB to NMS249, the blocking cysteine or glutathione that was present on the introduced cysteine was removed by reduction with 50-fold molar excess dithiothreitol (DTT) in Tris buffer overnight. Reducing agent was removed by diafiltration, and the interchain disulfide bonds were reformed by incubating the THIOMAB for 3 hours in 15-fold molar excess dhAA (dehydroascorbic acid; Sigma-Aldrich). The maleimide-linked NMS249 was incubated at 3- to 4-fold molar excess with the activated THIOMAB for 1 hour at 25°C. The antibody conjugate was purified using ion exchange chromatography (HiTrap S GE Healthcare Bio-Sciences) to remove excess NMS249. The ADC concentration was determined by BCA protein assay (Thermo Scientific Micro BCA Protein Assay Kit). The number of conjugated linker-drug molecules per mAb was calculated from the integrated UV peaks of the drug to antibody ratio (DAR) species resolved by analytical hydrophobic interaction chromatography (HIC; TSK butyl-NPR 4.6 mm × 10 cm, 2.5 μm; Tosoh Bioscience). The DAR was confirmed by analyzing the reduced and intact ADC by LC-MS (Agilent 9520 ESI Q-TOF, polymeric reversed-phase column PLRPS, 1000A, 8u). Molecular masses were derived from multiply charged ions deconvoluted using MassHunter software (Agilent Technologies).

Cell lines

The NHL cell lines BJAB.Luc, Granta-519, SuDHL4.Luc, and WSU-DLCL2 were obtained from the Genentech cell line repository. All cell lines were maintained in RPMI 1640 supplemented with 10% FBS (Sigma) and 2 mmol/L L-glutamine. Each cell line was authenticated by short tandem repeat (STR) profiling using the Promega PowerPlex 16 System and compared with external STR profiles of cell lines to determine cell line ancestry. In addition, an SNP fingerprint is generated from the original thaw to serve as our internal master fingerprint. The SNP fingerprinting is performed each time a new batch was frozen down. Cell lines were typically used for several months before thawing a new passage.

Target expression levels in xenograft tumors and cell lines

To measure the target expression on xenograft tumors, recovered tumors were minced and put through a 30 μm cell strainer (BD Biosciences) to achieve a single-cell suspension. The tumor cells were subsequently prepared by the standard density centrifugation over lymphocyte separation medium (MP Biomedicals). The resulting single-cell suspension was stained with anti-human CD22-APC antibody (BD Biosciences; clone S-HCL-1), anti-human CD79b-PE antibody (Beckman Coulter; clone CB3-1), anti-human CD20-Pacific Blue antibody (Beckerman Coulter; clone B9E9), and 7-amino-actinomycin D (BD Biosciences). Samples were acquired on FACSCalibur or LSR II flow cytometer (BD Biosciences). Data were analyzed using FlowJo (Tree Star), and the mean fluorescent intensity (MFI) was calculated from the $CD20^+$ and 7-amino-actinomycin D–negative population. CD22 and CD79b expression on cell lines was measured with the same set of antibodies.

Target internalization

To measure the CD22 internalization after antibody binding, cells were pre-equilibrated at 4°C with 10 μg/mL of same anti-CD22 antibody used in ADC for 30 minutes. Cells were then washed off excess unbound antibodies and put on ice (in PBS with azide) or incubated at 37°C (in cell culture media) for 1 hour. Afterward, cells were washed and stained with phycoerythrin (PE)-conjugated goat anti-human IgG antibody (Jackson ImmunoResearch) or rat anti-human kappa antibody (BD Biosciences). Samples were acquired on FACSCalibur, and analyzed using FlowJo. Percentage internalization was calculated as of [geoMFI (ice) – geoMFI(37°C)] / geoMFI(ice) × 100.

Cell viability assay

Cells were plated in triplicates at 10 to 20 × 10^3 per well in 96-well plates in RPMI containing 10% FBS overnight before treatment with test articles. Each test article was added to

experimental wells by nine-step 3-fold dilution, with control wells receiving medium alone. After 4-day incubation at 37°C, cell viability was measured using the PrestoBlue Cell Viability Reagent (Life Technologies). The concentration of test article resulting in the 50% inhibition of cell viability was calculated from a four-parameter nonlinear regression curve fit analysis by Prism (GraphPad Software).

P-gp inhibitor XR9051 (Tocris Bioscience), if used, was added 3 hours before treatment with test articles at a maximum concentration (400 nmol/L) that does not affect the normal cell growth.

Microarray and real-time PCR

Three biologic replicates were used for the parental cell lines (BJAB.Luc and WSU-DLCL2) and for the resistant lines (BJAB.Luc-22R1.1, BJAB.Luc-22R1.2, WSU-22R1.1, and WSU-22R1.2). Total RNA was extracted using the RNeasy plus mini Kit (QIAGEN). Complementary RNA was synthesized and hybridized to Affymetrix Human Genome U133 Plus 2.0 arrays.

To identify genes differentially expressed across all four resistant lines, a simplified linear model was used:

$$Y_{gs} \sim \beta_{0g} + \beta_{1g} X_{1s} + \beta_{2g} X_{2s} + \varepsilon_{gs},$$

where Y_{gs} is the expression value for gene "g" in sample "s"; β_{0g} is the (Intercept) expression in parental BJAB.Luc line; β_{1g} is the parental line-specific fixed effect; β_{2g} is the treatment-specific fixed effect; X_{1s} is the indicator variable for parental cell line (0: BJAB.Luc, 1: WSU-DLCL2); X_{2s} is the indicator variable for treatment (0: parental, 1: resistant); and ε_{gs} is the gene and sample-specific random error.

The treatment-specific effect was the effect of interest. The analysis was done using the "limma" (10) package from Bioconductor. The genes were then ranked by the *P* value for the treatment effect.

Real-time RT-PCR was performed on an ABI 7500 according to the manufacturer's instruction (Applied Biosystems), using the following primer sets. Mean threshold cycle (Ct) values were calculated to determine the fold differences.

ABCB1(P-gp)-forward	GTCCCAGGAGCCCATCCT
ABCB1(P-gp)-reverse	CCCGGCTGTTGTCTCCATA
ABCB1(P-gp)-probe	TGACTGCAGCATTGCTGAGAACATTGC
ABCC1-forward	TGGTGCCCGTCAATGCT
ABCC1-reverse	CGATTGTCTTTGCTCTTCATGTG
ABCC1-probe	ACCTGATACGTCTTGGTCTTCATCGCCA
ABCC3-forward	TCATCCTGGCGATCTACTTCCT
ABCC3-reverse	GTGGAATCAGCAAGACCATGAA
ABCC3-probe	CCCTCTGTCCTGGCTGGAGTCGC
ABCG2-forward	TTGGCTGTCATGGCTTCAGTAC
ABCG2-reverse	CCCAAAAATTCATTATGCTGCAA
ABCG2-probe	TCAGCATTCCACGATATGGATTTACGGC

In vivo efficacy xenograft experiments

Xenograft experiments were performed as previously described (10). Briefly, all animal studies were performed in compliance with NIH guidelines for the care and use of laboratory animals and were approved by the Institutional Animal Care and Use Committee (IACUC) at Genentech, Inc. Tumor cells (2×10^7 cells in 0.2 mL Hank's balanced salt solution) were inoculated subcutaneously into the flanks of female CB17 ICR SCID mice (Charles River Lab). When mean tumor size reached the desired volume, the mice were divided into groups of 7 to 10 mice with the same mean tumor size and dosed i.v. via the tail vein with ADCs. The results were plotted as mean tumor volume ± SEM of each group over time. Tumor stasis was defined as tumor volume unchanged from day 0. Partial regression was defined as tumor shrinkage of >50% but <100% of the initial tumor volume on day 0. Complete remission was defined as 100% tumor shrinkage (i.e., no detectable tumor) during the study. Tumor growth inhibition (TGI) was calculated as percent area under the tumor volume–time curve (AUC) per day of each treatment group in relation to the vehicle, using the following formula: $\%TGI = 100 \times [1 - (AUC_{treatment}/day \div AUC_{vehicle}/day)]$. To allow for comparison between groups across tumor models, the confidence intervals (CI) for %TGI were determined, and the 2.5 and 97.5 percentiles of CIs were reported as the lower and upper range of %TGI. The reported CIs were the values for which the recalculated values of %TGI would fall in this range 95% of the time. Groups with no overlapping CIs are considered significantly different from each other.

Development of anti-CD22-vc-MMAE–resistant cell lines

Two NHL models BJAB.Luc and WSU-DLCL2 were used to develop acquired resistance to anti-CD22-vc-MMAE. Tumor cells were inoculated subcutaneously into the flanks of female CB17 SCID mice. When tumors reached 200 to 500 mm^3 in size, mice received an initial intravenous dose of anti-CD22-vc-MMAE to drive partial tumor regression.

Mice were dosed again when tumors regrew from the treatment (i.e., tumors grew back to the initial tumor volume at day 0). Dose levels were slowly increased each time until it reached 10× above the initial dose or MTD in mice. Frequency of doses administered varied over time based on the rate of tumor regrowth, but did not exceed 2 doses/week. The range of doses administered for BJAB.Luc model was 1.5, 2, 2.5, 3, 3.5, 4, 5, 6, 8, 15, and 20 mg/kg, and the range of doses for WSU-DLCL2 model was 12, 15, 18, 20, 25, and 30 mg/kg. Dosing was discontinued once a tumor was no longer responding to a series of increasing doses. Tumors were then collected and put back in culture to generate resistant cell lines for further characterization. Two resistant cell lines for each tumor model were successfully established and named as BJAB.Luc-22R1.1, BJAB.Luc-22R1.2, WSU-22R1.1, and WSU-22R1.2.

Generation of P-gp overexpressing cell line

P-gp expression vector was a kind gift from Jun Guo, Genentech. BJAB.Luc cells were transfected with either pIRES-hrGFP II control vector (Agilent Technologies) or the P-gp expression vector. The transfectants were selected under Geneticin (Life Technologies) and sorted with anti-P-gp antibody to acquire the highest expressing clone as determined by flow cytometry. For surface detection of P-gp, cells were incubated for 30 minutes on ice with PE-labeled anti–P-gp antibody (eBioscience; clone UIC2) or a PE-labeled isotype-negative control. Cells were washed with cold PBS and analyzed by standard flow cytometry.

P-gp functional assay via Rhodamine 123

Approximately 10^6 cells were prepared in PBS buffer with 500 ng/mL of Rhodamine 123 (Life Technologies) and incubated at

Table 1. *In vitro* potency of free drugs and CD22-ADCs

IC_{50} (95% CI)	BJAB.Luc	Granta-519	SuDHL4.Luc	WSU-DLCL2
MMAE (nmol/L)	0.54 (0.49–0.60)	0.25 (0.23–0.27)	1.19 (1.15–1.22)	0.25 (0.24–0.27)
PNU-159682 (nmol/L)	0.10 (0.09–0.11)	0.020 (0.018–0.023)	0.055 (0.050–0.060)	0.1[a]
control-vc-MMAE (μg/mL)	>10	>10	>10	>10
anti-CD22-vc-MMAE (μg/mL)	1.1 (1.0–1.3)	0.55 (0.45–0.68)	0.95 (0.85–1.06)	0.014 (0.013–0.015)
control-NMS249 (μg/mL)	2.4 (1.4–4.0)	1.96 (1.88–2.04)	2.88 (2.84–2.92)	1.9 (1.7–2.3)
anti-CD22-NMS249 (μg/mL)	0.058 (0.056–0.059)	0.030 (0.027–0.032)	0.0221 (0.0217–0.0225)	0.010 (0.095–0.012)

[a]Curve fit was ambiguous, CI value was too wide to report.

room temperature for 30 minutes. Subsequently, cells were washed twice with RPMI media and divided into 3 tubes, one tube was placed immediately on ice to serve as the baseline uptake, the second tube was incubated for 2 hours at 37°C, and the third one was pretreated with 400 nmol/L of P-gp inhibitor XR9051 before incubated at 37°C. Afterwards, test tubes were put on ice to stop the reaction; samples were washed twice with ice-cold PBS, and analyzed by flow cytometry.

Results

Generation and characterization of NMS249 ADCs

Anthracyclines are broadly used in the treatment of cancer, and efforts have been made to make anthracycline analogues that increase the effectiveness and safety for this class of drug. One of those analogues, Nemorubicin [(3′-deamino-3′-[2″(S)-methoxy-4″-morpholinyl]doxorubicin; MMDX], was selected for clinical evaluation because it was not cardiotoxic at doses that were effective in multidrug-resistant tumor models (12). PNU-159682 was identified as a metabolic product of nemorubicin that was 700- to 2,400-fold more potent in *in vitro* cytotoxicity assays than nemorubicin (13) with picomolar IC_{50}s. Our cell viability assay data were consistent with this observation, and we observed that PNU-159682 was more potent than MMAE on our model NHL cell lines in two cases by an order of magnitude or more (Table 1).

We were interested to see if we could develop an effective anthracycline-based ADC using PNU-159682. Given the complexity of ADC development, we selected other components of the ADC that have prior clinical validation and existing preclinical tools and data. We selected the clinically validated linker maleimidocaproyl-valine-citrulline-p-aminobenzoyloxycarbonyl (MC-vc-PAB) used in pinatuzumab vedotin and polatuzumab vedotin and the approved ADC brentuximab vedotin [anti-CD30-MC-vc-PAB-monomethyl auristatin E (MMAE)] and attached it to the primary alcohol of PNU-159682 through a diethylamine (DEA) linkage to make the linker-drug MC-vc-PAB-DEA-PNU-159682 (referred to henceforth as NMS249; Fig. 1A). For the antibody, we choose the same anti-CD22 antibody in pinatuzumab that is in clinical development as an MC-vc-PAB-MMAE ADC (pinatuzumab vedotin, DCDT2980S, anti-CD22-MC-vc-PAB-MMAE). However, to control drug load, we have engineered an cysteine residue into the IgG heavy chain (HC-A114C) that provides two reactive thiols for conjugation to maleimide-based linkers (11). This site-specific conjugation results in nearly homogenous conjugation of two drugs per antibody (Fig. 1B and C). This ADC, Thio-anti-CD22(10F4v3)-NMS249 (referred to from here on as anti-CD22-NMS249), was

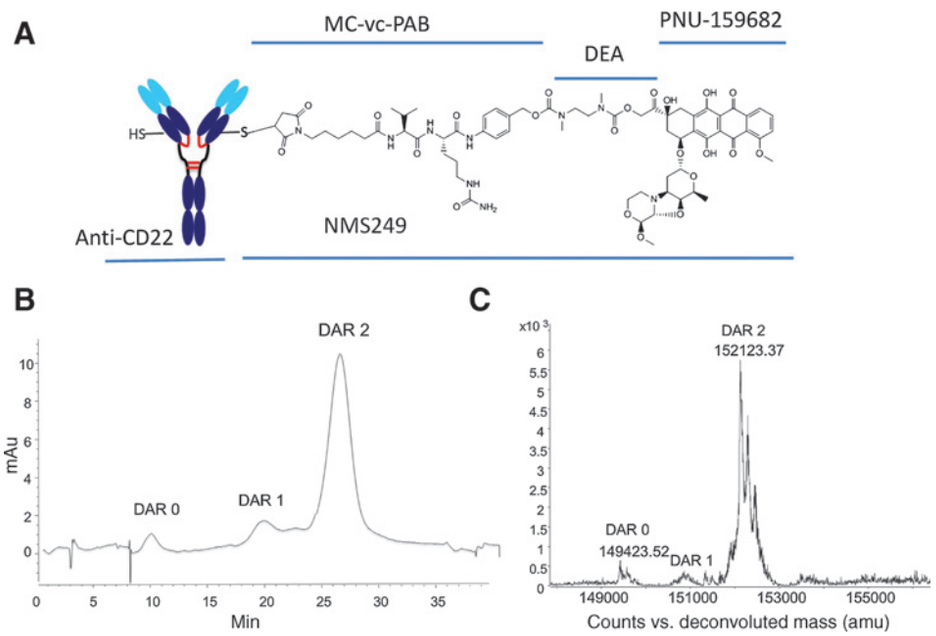

Figure 1.
Description of NMS249 ADCs. A, structure of NMS249 ADCs. Only one NMS249 attached to a cysteine engineered in to the antibody heavy chain is shown for clarity. B, HIC chromatogram of anti-CD22-NMS249 showing relative distribution of DAR. C, deconvoluted LC-MS chromatogram of intact anti-CD22-NMS249.

active in *in vitro* viability assays of NHL cell lines and was 2- to 20-fold more potent than pinatuzumab vedotin (anti-CD22-MC-vc-PAB-MMAE, referred to from here on as anti-CD22-vc-MMAE) despite having a lower drug load (Table 1).

In vivo efficacy of anti-CD22-NMS249 ADC

We sought evidence that anti-CD22-NMS249 could be effective *in vivo*. We tested the tolerability of the ADC in mice and found that a single 2 mg/kg ADC dose (50 μg/m^2 conjugated PNU-159682) was well tolerated resulting in less than 10% weight loss. We tested four xenograft models and found that anti-CD22-NMS249 was active in all four models (Fig. 2). First two of the xenograft models, BJAB.luc and WSU-DLCL2, represented the extremes of sensitivity to the auristatin-based conjugates. BJAB.Luc is very sensitive to anti-CD22-vc-MMAE and anti-CD79b-vc-MMAE whereas WSU-DLCL2 relatively insensitive to both conjugates (ref. 5; Supplementary Figs. S1 and S2). In the BJAB.Luc model, the efficacy of anti-CD22-NMS249 (Fig. 2A) was similar to anti-CD22-vc-MMAE (Supplementary Fig. S1A), where a single dose of 2 mg/kg gives complete remission of the tumors (NMS249: 110–134%TGI vs. vc-MMAE: 114–143%TGI). However in the more resistant WSU-DLCL2 model, anti-CD22-NMS249 was more effective. A single dose of anti-CD22-NMS249 at 2 mg/kg resulted in tumor stasis for 3 weeks (Fig. 2B; 99–125%TGI), where anti-CD22-vc-MMAE requires a dose of 8 mg/kg to achieve similar efficacy (ref. 5; Supplementary Fig. S2A; 109–170%TGI). To further evaluate the activity of anti-CD22-NMS249, we tested it in two additional xenograft models, Granta-519 and SuDHL4.Luc, and found that anti-CD22-NMS249 was very effective in

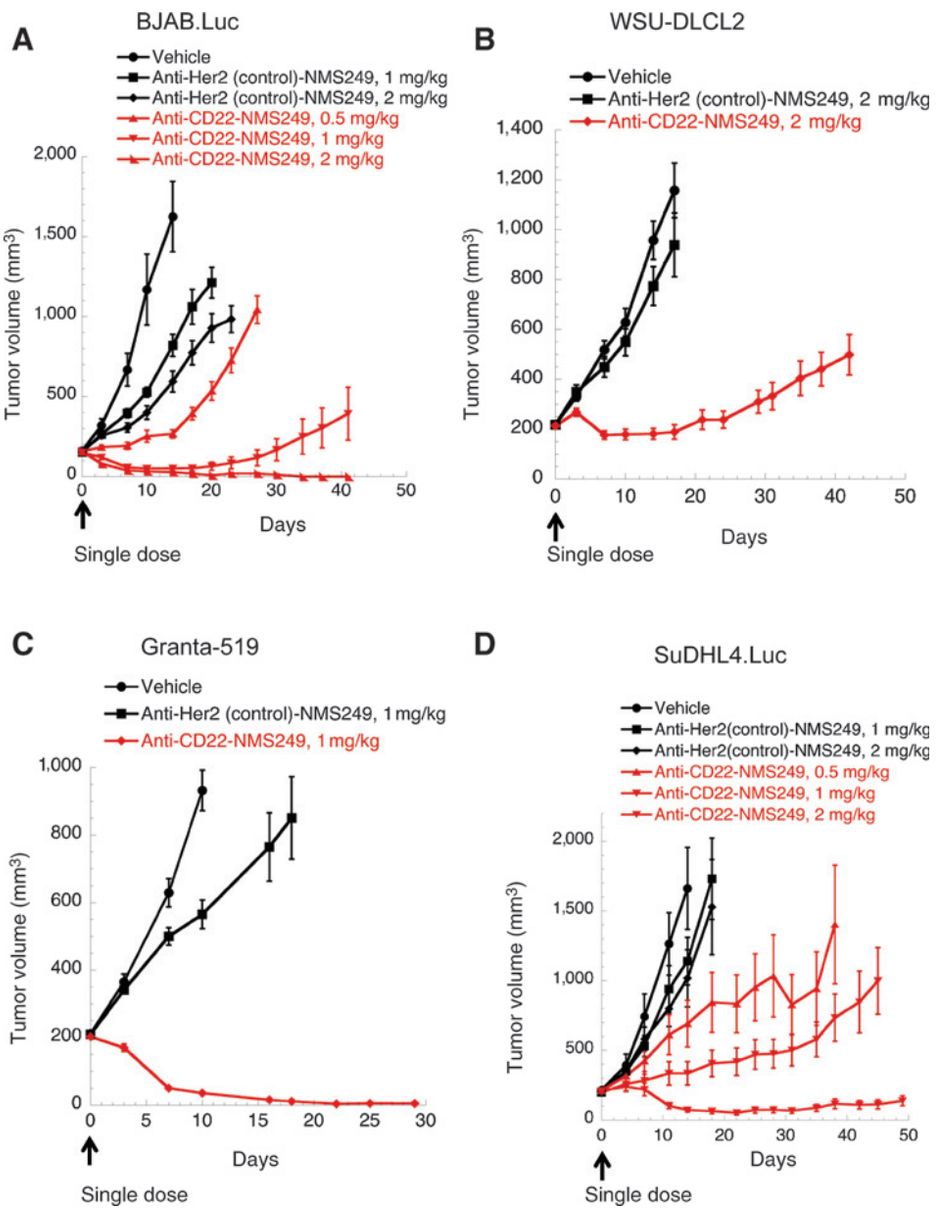

Figure 2.
In vivo efficacy of anti-CD22-NMS249 in tumor xenograft models of (A) BJAB.Luc Burkitt's lymphoma, (B) WSU-DLCL2 diffuse large B-cell lymphoma, (C) Granta-519 mantle-cell lymphoma, and (D) SuDHL4.Luc diffuse large B-cell lymphoma. Group mean (±SEM) tumor volumes over the duration of the study are shown for animals administered with a single i.v. dose of vehicle, anti-Her2-NMS249 (negative control), or anti-CD22-NMS249 at 0.5, 1, or 2 mg/kg. SCID mice were subcutaneously implanted with 20 million tumor cells, and dosed (as indicated by arrow) when average tumor size reached 150 to 220 mm^3 (n = 7–9 mice/group).

these models as well (Fig. 2C and D). A single dose anti-CD22-NMS4249 at 1 mg/kg caused sustained complete remission of Granta-519 tumors (121–145%TGI), and a single dose at 2 mg/kg drove partial regression of SuDHL4.Luc tumors (95–129%TGI). These data show that our anthracycline-based ADC can be effective *in vivo* across multiple models of NHL. However, the apparent great increase in potency of anti-CD22-NMS249 compared with anti-CD22-vcMMAE observed *in vitro* was less pronounced in the corresponding xenograft models.

Development and characterization of cell lines resistant to anti-CD22-vc-MMAE

We were interested in the observation that anti-CD22-NMS249 was comparatively more effective in the model that was less responsive to the microtubule inhibitor–based ADCs. To further explore this and to try to understand the factors that might confer resistance to the anti-CD22-vc-MMAE ADC (currently in clinical testing), we developed BJAB.Luc and WSU-DLCL2 models that were resistant to anti-CD22-vc-MMAE. To achieve this, we treated the xenograft models with a dose of anti-CD22-vc-MMAE that caused partial tumor regression. Upon regrowth of the tumor, the mice were treated again with a higher dose. This procedure was repeated until the tumors continued to grow despite exposure to relatively high levels of anti-CD22-vc-MMAE, and then tumors were removed and cultured *in vitro*. These newly derived cell lines (BJAB.Luc-22R1.1, BJAB.Luc-22R1.2, and WSU-22R1.1, WSU-22R1.2) were resistant to anti-CD22-vc-MMAE and anti-CD79b-vc-MMAE conjugates and to free MMAE *in vitro* (Supplementary Fig. S3). The *in vitro* resistance was not due to reduction in target levels (data not shown) or internalization efficiency (Supplementary Fig. S3D) as determined by flow cytometry. We tested two of the cell lines *in vivo* for resistance to anti-CD22-vc-MMAE and anti-CD79b-vc-MMAE conjugates. When the BJAB.Luc-22R1.2 and WSU-22R1.1 cell lines were grown as xenograft tumors, they were resistant to both anti-CD22-vc-MMAE and anti-CD79b-vc-MMAE conjugates (Fig. 3A and B); at the dose levels that caused regression of the corresponding parental tumors (Supplementary Fig. S1; 4 mg/kg CD22 or CD79b: 116–150%TGI and 116–137%TGI, respectively, and Supplementary Fig. S2; 8 mg/kg CD22 or 4 mg/kg CD79b: 109–170%TGI and 103–144%TGI, respectively), the growth of the resistant cell lines was barely delayed (Fig. 3A; 8 mg/kg CD22 or CD79b: −28–43%TGI and 74–96%TGI, respectively, and Fig. 3B; 12 mg/kg CD22 or CD79b: 11–49%TGI and 47–73%TGI, respectively). Again, this was not due to target modulation, as CD22 and CD79b maintained their expression in the resistant xenograft tumors (Fig. 3C).

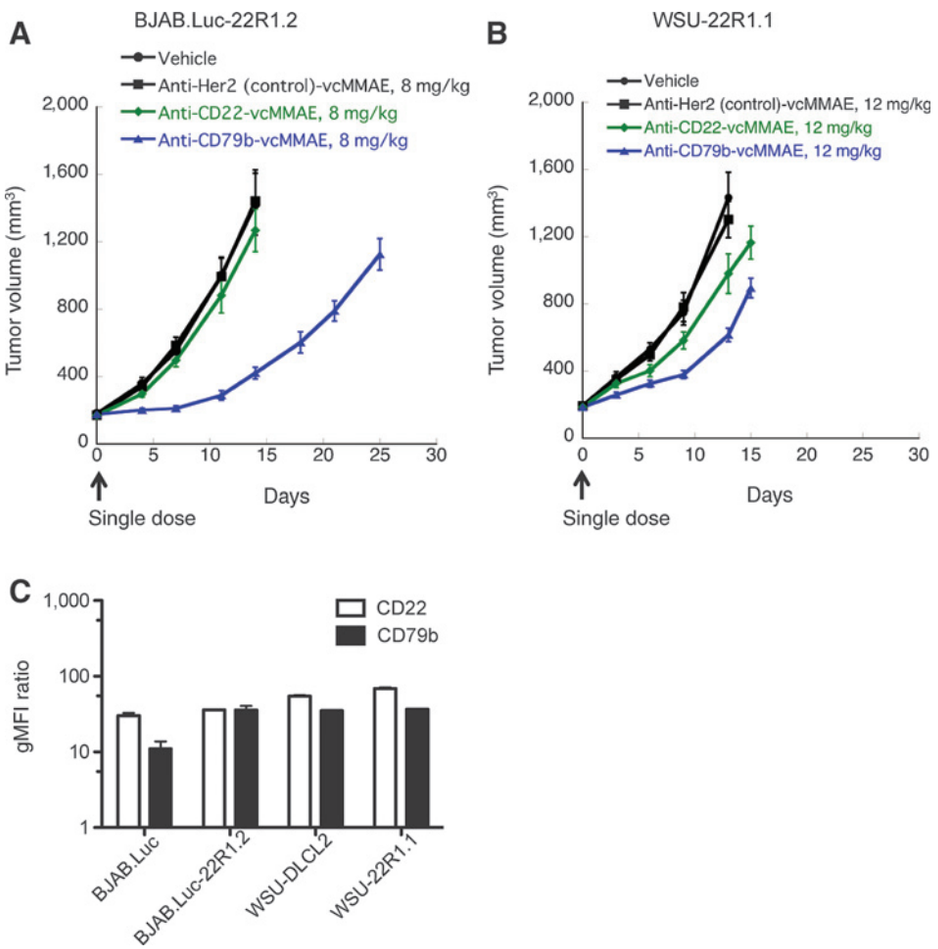

Figure 3.
Tumor xenograft models with acquired resistance to anti-CD22-vc-MMAE were also less responsive to anti-CD79b-vc-MMAE. Group mean (±SEM) tumor volumes over the duration of the study are shown for animals administered with a single i.v. dose of vehicle, anti-Her2-vc-MMAE (negative control), anti-CD22-vc-MMAE, or anti-CD79b-vc-MMAE (A and B). A, subcutaneous xenograft tumors of Burkitt's lymphoma (BJAB.Luc-22R1.2, 20 million cells/mouse) were allowed to grow to an average 175 mm^3 and then dosed with 8 mg/kg ADCs ($n = 9$/group). B, subcutaneous xenograft tumors of diffuse large B-cell lymphoma (WSU-22R1.1, 20 million cells/mouse) were allowed to grow to an average 190 mm^3 and then dosed with 12 mg/kg ADCs ($n = 8$/group). C, the level of surface CD22 and CD79b expression on dissociated xenograft tumor cells as assayed by flow cytometry.

Table 2. Top 10 differentially expressed genes between anti-CD22-vc-MMAE–resistant lines and parental cell lines

	Probe	Entrez	Symbol	Gene name	BJAB.Luc-22R1.1 Fold change	BJAB.Luc-22R1.2 Fold change	WSU-22R1.1 Fold change	WSU-22R1.2 Fold change
1	209993_at	5243	*ABCB1*	ATP-binding cassette, sub-family B (MDR/TAP), member 1	65.2	263	109	68.3
	243951_at	5243	*ABCB1*	ATP-binding cassette, sub-family B (MDR/TAP), member 1	8.34	36.8	16.9	14.3
2	212623_at	440026	*TMEM41B*	Transmembrane protein 41B	1.73	1.57	1.97	1.41
	212622_at	440026	*TMEM41B*	Transmembrane protein 41B	1.49	1.48	1.89	1.41
3	208955_at	1854	*DUT*	Deoxyuridine triphosphatase	−1.59	−1.32	−1.44	−1.22
4	226882_x_at	10785	*WDR4*	WD repeat domain 4	−1.25	−1.26	−1.5	−1.5
5	235467_s_at	3749	*KCNC4*	Potassium voltage-gated channel, Shaw-related subfamily, member 4	−1.4	−1.36	−1.63	−1.68
6	214102_at	116984	*ARAP2*	ArfGAP with RhoGAP domain, ankyrin repeat, and PH domain 2	−1.5	−1.27	−2.28	−1.81
7	212561_at	23258	*DENND5A*	DENN/MADD domain containing 5A	1.48	1.71	2.15	1.82
8	217981_s_at	26515	*FXC1*	Fracture callus 1 homolog (rat)	1.45	1.6	1.47	1.22

NOTE: Only genes with an absolute fold change of 1.5 or above and a false-discovery rate less than 0.05, in at least one cell line, are shown.

We compared the resistant and parental cell lines by oligonucleotide microarray to look for the modulation of gene expression across all four resistant cell lines. *P-gp (ABCB1/MDR1)* was the only gene upregulated by at least one order of magnitude (Table 2). None of the remaining differentially expressed genes had changes more than 2-fold across all four cell lines examined. Real-time PCR analysis further verified that among four multi-drug resistant genes (*ABCB1/P-gp*, *ABCC1/MRP1*, *ABCC3/MRP3*, and *ABCG2/BCRP1*) tested, only the *ABCB1/P-gp* gene was significantly overexpressed (data not shown). We further confirmed the upregulation of P-gp by flow cytometry (Fig. 4A) and efflux function assay with Rhodamine 123 (Fig. 4B). Both BJAB.Luc-22R1.2 and WSU-22R1.1 cell lines had surface expression of P-gp protein by approximately a 100-fold over the parental cell lines. In addition, both cell lines lost the ability to retain Rhodamine 123 signal, indicating an active efflux mediated by P-gp. Those two cell lines regained their Rhodamine 123 signal after treatment of P-gp inhibitor, further demonstrating the functionality of P-gp.

To confirm that the P-gp was the major driver of resistance, we made a stably transfected P-gp overexpressing BJAB cell line (BJAB.Luc-P-gp) and tested efficacy of the ADCs in that cell line. The P-gp–transfected cell line expressed a similar level of surface P-gp as the resistant cell lines (Fig. 4A), and became resistant to the treatment of anti-CD22-vc-MMAE and anti-CD79b-vc-MMAE, as well as to free drug MMAE *in vitro* (Supplementary Fig. S4). This acquired resistance can be completely reversed by pretreating the cells with the P-gp inhibitor XR9051 (Supplementary Fig. S4). We next characterized the P-gp stably expressing BJAB.Luc-P-gp model as xenografts in mice, and confirmed that this model also showed resistance *in vivo* to anti-CD22 and anti-CD79b vc-MMAE conjugates (Fig. 5A; 8 mg/kg CD22 or CD79b: 27–64%TGI and 40–75%TGI, respectively, vs. Supplementary Fig. S1; 4 mg/kg CD22 or CD79b: 116–150%TGI and 116–137%TGI, respectively).

Efficacy of anti-CD22-NMS249 in cell lines resistant to anti-CD22-vc-MMAE

We were interested to know whether switching the payload of the ADC to PNU-159682 could overcome the

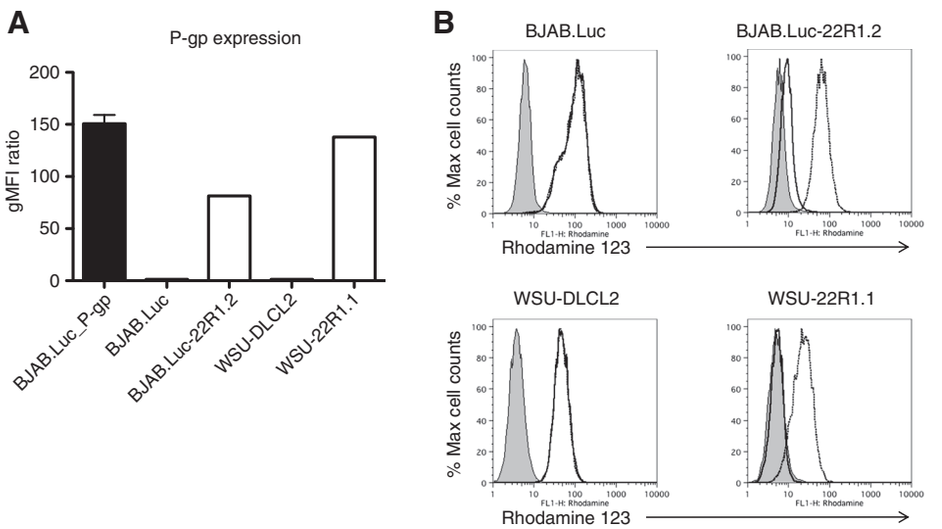

Figure 4.
The acquired resistance to anti-CD22-vc-MMAE was due to the overexpression of P-gp. A, the level of surface P-gp expression on resistant cell lines as assayed by flow cytometry. B, efflux functional assay via Rhodamine 123. Each panel shows the Rhodamine 123 signal from the cells untreated (solid line) or treated with P-gp inhibitor (dotted line), overlaid with isotype control (gray histogram). In contrast with parental cell lines, Rhodamine 123 signal was greatly reduced in two tumor-derived resistant cell lines indicating the active efflux mediated by P-gp, and the reduction could be reversed after treating with P-gp inhibitor.

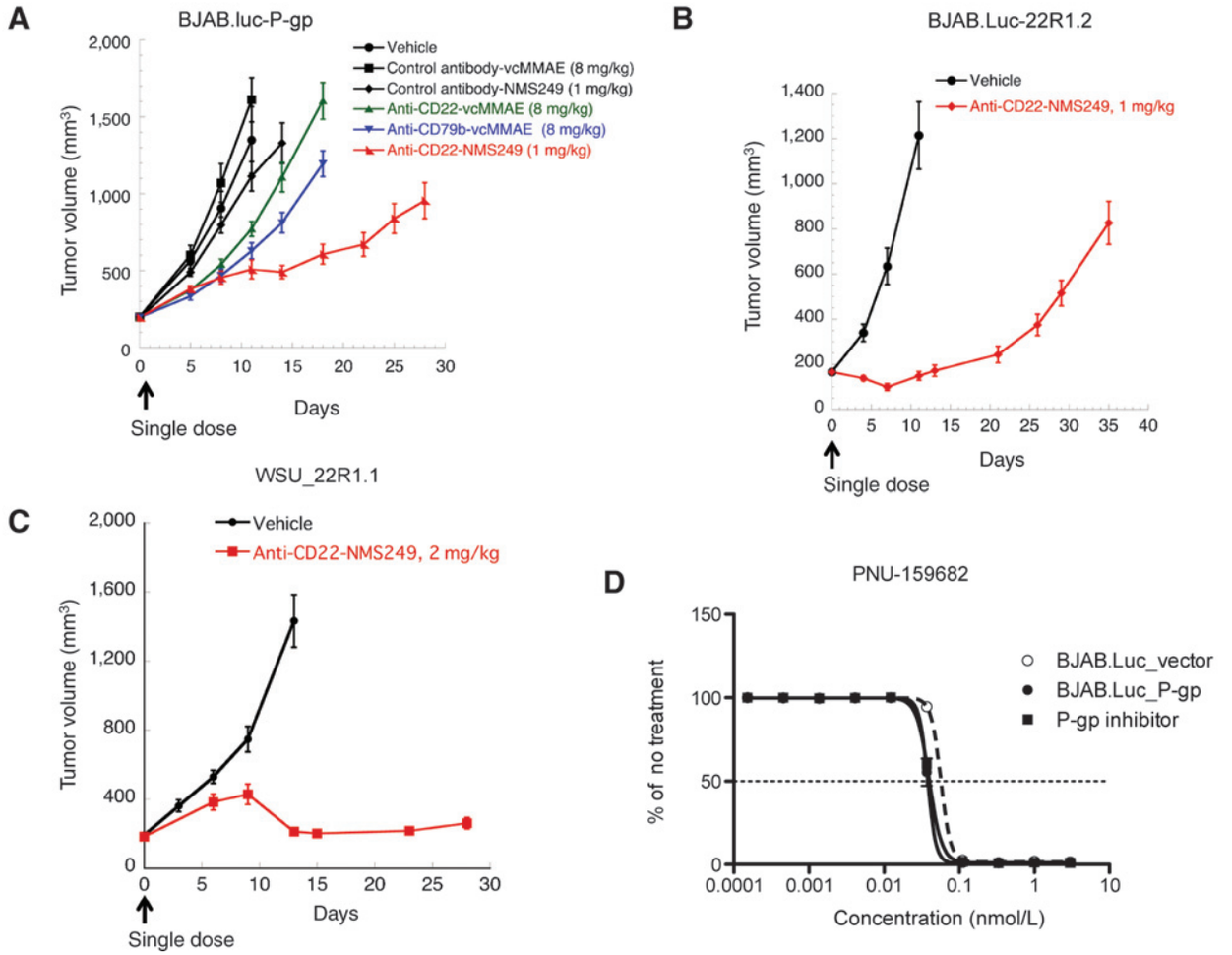

Figure 5.
In vivo efficacy of anti-CD22-NMS249 in tumor xenograft models with resistance to anti-CD22-vc-MMAE. A, subcutaneous xenograft tumors of over-expressing P-gp (BJAB.Luc-P-gp, 20 million cells/mouse) were allowed to grow to an average 197 mm^3 and then dosed with vehicle, anti-Her2-vc-MMAE (negative control), anti-CD22-vc-MMAE, anti-CD79b-vc-MMAE at 8 mg/kg, anti-Her2-NMS249 (negative control), or anti-CD22-NMS249 at 1 mg/kg ($n = 8$/group). B, subcutaneous xenograft tumors of Burkitt's lymphoma (BJAB.Luc-22R1.2, 20 million cells/mouse) were allowed to grow to an average 166 mm^3 and then dosed with 1 mg/kg anti-CD22-NMS249 ($n = 8$/group). C, subcutaneous xenograft tumors of diffuse large B-cell lymphoma (WSU-22R1.1, 20 million cells/mouse) were allowed to grow to an average 189 mm^3 and then dosed with 2 mg/kg anti-CD22-NMS249 ($n = 8$/group). D, P-gp over-expressing cell line BJAB.Luc_P-gp had the same response to free PNU-159682 as the cell line expressing the control vector.

resistance to vc-MMAE ADCs. We tested the efficacy of anti-CD22-NMS249 in the BJAB.Luc-22R1.2– and WSU-22R1.1–induced resistant cell lines and the P-gp overexpressing cell line BJAB.Luc-P-gp *in vivo* and found that anti-CD22-NMS249 maintained its most or all of its efficacy in the xenograft models (Fig. 5A–C). A single dose anti-CD22-NMS249 (at 1 mg/kg in BJAB.Luc-22R1.2 or at 2 mg/kg in WSU-22R1.1) resulted in tumor stasis for at least 3 weeks (104–118%TGI in BJAB.Luc-22R1.2 and 56–79%TGI in WSU-22R1.1). A single dose at 1 mg/kg in BJAB.Luc-P-gp also resulted in prolonged TGI. The active compound released from the NMS249 linker drug has not been identified. However, because PNU-159682 is not a substrate for P-gp (Fig. 5D), a simple explanation for efficacy of anti-CD22-NMS249 is that the active compound released in cells is a poor P-gp substrate.

Discussion

We describe an anti-CD22 ADC with an anthracycline as the chemotherapeutic payload. As part of this work, we developed anti-CD22-vc-MMAE–resistant cell lines that were resistant to anti-CD79b-vc-MMAE as well. We show that the major, if not the only, driver of this acquired resistance is overexpression of P-gp. The amount of active P-gp can be difficult to assess in clinical samples; however, it seems clear that P-gp levels have some role in the resistance to chemotherapy and overall survival of NHL patients, although the extent of that role is controversial (14, 15). It is unclear how much P-gp is a driver of resistance to the vc-MMAE–based ADCs in the clinic, but our data show that it has that potential. Our anthracycline-based ADC can overcome the resistance driven by P-gp presumably because the released active drug is a poor substrate for P-gp.

Consistent with this idea, the free drug, PNU-159682, is not a P-gp substrate (Fig. 5D).

The WSU-DLCL2 xenograft model was less sensitive to the microtubule inhibitor–based ADCs (Supplementary Fig. S2), including both vc-MMAE and SPDB-DM4 conjugates. What drives this unresponsiveness is unknown. It was not due to target levels as the model has equal or higher expression of CD22 than BJAB.Luc (5), or the internalization efficiency as WSU-DLCL2 has a higher internalization rate than BJAB.Luc (Supplementary Fig. S3D). *In vitro* sensitivity of these two cell lines to free drug is also very close (Table 1 ref. 5). However, we observed that in this model, anti-CD22-NMS249 has shown a much better improvement on efficacy. This could be because NMS249 is a more potent linker drug and its potency is only revealed in resistant models or that the different mechanism of action changes the relative sensitivities of the cell lines. In any case, our data suggest that regardless of P-gp expression, our anthracycline-based ADC has the potential to be more effective in patients who do not respond to the MMAE-based ADCs currently in the clinic.

ADCs offer the promise of increased therapeutic index for chemotherapy and possibly could replace systemic chemotherapies of the same mechanism. This strategy is being tried for the treatment of systemic anaplastic large cell lymphoma where the vincristine in the standard of care CHOP (cyclophosphamide, doxorubicin, vincristine, prednisone) combination chemotherapy is removed and replaced with the ADC Brentuximab Vedotin (anti-CD30-vc-MMAE) that has the same mechanism of action. Having an ADC based on an anthracycline would open up the possibility of replacing the anthracycline in cancers where it is current standard of care.

Disclosure of Potential Conflicts of Interest

R. Cohen is an employee of Calico Life Sciences. J. Flygare is an employee of and holds ownership interest (including patents) in Roche. A.G. Polson holds ownership interest (including patents) in Roche/Genentech. No potential conflicts of interest were disclosed by the other authors.

Authors' Contributions

Conception and design: S.-F. Yu, B. Zheng, R. Cohen, J. Flygare, A.G. Polson
Development of methodology: S.-F. Yu, B. Zheng
Acquisition of data (provided animals, acquired and managed patients, provided facilities, etc.): S.-F. Yu, B. Zheng, M. Go, J. Lau, H. Raab
Analysis and interpretation of data (e.g., statistical analysis, biostatistics, computational analysis): S.-F. Yu, B. Zheng, M. Go, J. Lau, S. Jhunjhunwala, J. Flygare, A.G. Polson
Writing, review, and/or revision of the manuscript: S.-F. Yu, B. Zheng, S. Spencer, P. Polakis, A.G. Polson
Administrative, technical, or material support (i.e., reporting or organizing data, constructing databases): S.-F. Yu, R. Soriano
Study supervision: S.-F. Yu, S. Spencer
Other (synthesis of drug): M. Caruso

Acknowledgments

The authors thank the *in vivo* cell culture lab at Genentech for developing resistance cell lines and preparing the cells for all the *in vivo* studies.

The costs of publication of this article were defrayed in part by the payment of page charges. This article must therefore be hereby marked *advertisement* in accordance with 18 U.S.C. Section 1734 solely to indicate this fact.

Received August 6, 2014; revised December 4, 2014; accepted April 2, 2015; published OnlineFirst April 3, 2015.

References

1. Senter PD. Potent antibody drug conjugates for cancer therapy. Curr Opin Chem Biol 2009;13:235–44.
2. Sievers EL, Senter PD. Antibody-drug conjugates in cancer therapy. Annu Rev Med 2013;64:15–29.
3. Chu YW, Polson A. Antibody-drug conjugates for the treatment of B-cell non-Hodgkin's lymphoma and leukemia. Future Oncol 2013;9:355–68.
4. Kreitman RJ, Pastan I. Antibody fusion proteins: anti-CD22 recombinant immunotoxin moxetumomab pasudotox. Clin Cancer Res 2011; 17:6398–405.
5. Li D, Poon KA, Yu SF, Dere R, Go M, Lau J, et al. DCDT2980S, an anti-CD22-monomethyl auristatin E antibody-drug conjugate, is a potential treatment for non-Hodgkin lymphoma. Mol Cancer Ther 2013;12:1255–65.
6. Palanca-Wessels MC, Flinn IW, Sehn LH, Patel M, Sangha R, Czuczman MS, et al. A phase I study of the anti-CD79b antibody-drug conjugate (ADC) DCDS4501A targeting CD79b in relapsed or refractory B-cell non-Hodgkin's lymphoma (NHL). ASH Annual Meeting Abstracts 2012;120:56.
7. Advani R, Lebovic D, Brunvand M, Chen AI, Goy A, Chang JE, et al. A phase I study of DCDT2980S, an Antibody-Drug Conjugate (ADC) targeting CD22, in relapsed or refractory B-cell non-Hodgkin's lymphoma (NHL). ASH Annual Meeting Abstracts 2012;120:59.
8. Younes A, Kim S, Romaguera J, Copeland A, Farial Sde C, Kwak LW, et al. Phase I multidose-escalation study of the anti-CD19 maytansinoid immunoconjugate SAR3419 administered by intravenous infusion every 3 weeks to patients with relapsed/refractory B-cell lymphoma. J Clin Oncol 2012;30:2776–82.
9. Ribrag V, Dupuis J, Tilly H, Morschhauser F, Laine F, Houot R, et al. A dose-escalation study of SAR3419, an anti-CD19 antibody maytansinoid conjugate, administered by intravenous infusion once weekly in patients with relapsed/refractory B-cell non-Hodgkin lymphoma. Clin Cancer Res 2014; 20:213–20.
10. Dornan D, Bennett F, Chen Y, Dennis M, Eaton D, Elkins K, et al. Therapeutic potential of an anti-CD79b antibody-drug conjugate, anti-CD79b-vc-MMAE, for the treatment of non-Hodgkin lymphoma. Blood 2009;114:2721–9.
11. Junutula JR, Raab H, Clark S, Bhakta S, Leipold DD, Weir S, et al. Site-specific conjugation of a cytotoxic drug to an antibody improves the therapeutic index. Nat Biotechnol 2008;26:925–32.
12. Sessa C, Valota O, Geroni C. Ongoing phase I and II studies of novel anthracyclines. Cardiovasc Toxicol 2007;7:75–9.
13. Quintieri L, Geroni C, Fantin M, Battaglia R, Rosato A, Speed W, et al. Formation and antitumor activity of PNU-159682, a major metabolite of nemorubicin in human liver microsomes. Clin Cancer Res 2005;11: 1608–17.
14. Rund D. Multidrug resistance in lymphoma: is it time for clinical trials? Leuk Lymphoma 2007;48:643–4.
15. Sandor V, Wilson W, Fojo T, Bates SE. The role of MDR-1 in refractory lymphoma. Leuk Lymphoma 1997;28:23–31.